Proceedings of the 5th International Conference on Materials Chemistry and Environmental Engineering
DOI: 10.54254/2755-2721/2025.23742

Study on Large-Scale Traveling Ionospheric Disturbances During the March 2023 Geomagnetic Storm in the North American and European Sectors

Zhesong Zheng

Chang'an University, Xi'an, China
2021126011@chd.edu.cn

Abstract: Using global Total Electron Content (TEC) data provided by the Madrigal database, this study investigates large-scale traveling ionospheric disturbances (LSTIDs) observed in the North American and European sectors during the geomagnetic storm on March 23, 2023. A second-order polynomial fitting method was applied to filter residuals, calculate ionospheric disturbance values, and create two-dimensional TEC disturbance maps showing variations across latitude and longitude. The results indicate the observation of multiple LSTIDs originating from the Arctic in both the European and North American sectors. Intense LSTIDs were found to propagate during the daytime in these sectors. In the North American sector, LSTIDs exhibited propagation speeds ranging from 512 to 610 m/s, while in the European sector, the speeds ranged from 575 to 652 m/s. The wave propagation direction in the North American sector averaged approximately 15 degrees southeast of south, whereas in the European sector, the average direction was 15 degrees southwest of south.

Keywords: Large-scale traveling ionospheric disturbances, geomagnetic storm, total electron content

1. Introduction

Traveling Ionospheric Disturbances (TIDs) are significant dynamic processes in the ionosphere, characterized by wave-like disturbances that cause corresponding variations in ionospheric parameters such as Total Electron Content (TEC). Over the past decades, TIDs have been widely studied [1-7] and are considered the ionospheric response to gravity waves in the thermosphere. Under specific space weather conditions, such as during geomagnetic storms, auroral oval heating in the polar regions is regarded as one of the key factors generating gravity waves, which in turn trigger large-scale TIDs. Investigating TIDs in depth is crucial for uncovering the coupling mechanisms between the magnetosphere, ionosphere, and thermosphere.

The widespread deployment of Global Positioning System (GPS) receivers worldwide has provided excellent opportunities for continuous TEC observations. In 1998, Saito et al. [8] utilized approximately 1,000 GPS receivers to analyze medium-scale TIDs over Japan and generated two-dimensional maps of TEC disturbances. Since then, GPS-based methods for analyzing disturbed TEC data have been widely applied in TID research, significantly advancing the understanding of TID phenomena. For instance, Tsugawa et al. conducted statistical studies on large-scale TIDs (LSTIDs) over Japan using GPS [9]. They reported that the attenuation of LSTIDs is associated with the angle

DOI: 10.54254/2755-2721/2025.23742

between their propagation azimuth and the geomagnetic field direction, identifying ion drag as the primary cause of LSTID attenuation in the region. To further understand the sources of TID disturbances, Ding Feng et al. performed statistical analyses of LSTIDs during geomagnetic storms in the high-latitude North American region using GPS data [10, 11]. Their findings revealed that the movement of auroral electrojet enhancement zones in high-latitude regions is a critical mechanism responsible for phase shifts in the disturbance wavefronts. In mid- to low-latitude regions, Song Qian et al. conducted a 2013 study using GPS data from China to investigate LSTIDs [12]. They concluded that LSTID propagation in these areas is influenced by factors such as background neutral atmospheric wind fields and equatorial electrojet activity.

Despite significant progress in the study of TIDs, substantial variability in TIDs characteristics remains due to differences in the magnetospheric, ionospheric, and thermospheric background conditions under which different TIDs events occur. This variability leads to notable differences in TIDs phenomena across events. For example, Zhang Shunrong et al. [13] reported that the source region of polar TIDs disturbances does not align with the commonly assumed nightside auroral zone. Their study identified cases of wavefronts exceeding 2000 km in length, propagating along transpolar paths from the dayside to the nightside. These findings underscore the necessity of conducting case studies to improve the understanding of various TIDs events.

The geomagnetic storm in March 2023 provided a valuable opportunity to study TIDs during geomagnetic disturbances. This study aims to perform a case analysis of the morphological characteristics of LSTIDs during this geomagnetic storm using high temporal and spatial resolution GPS TEC data from the American and European sectors.

2. Data and processing methods

2.1. Data description

This study primarily analyzes vertical Total Electron Content (TEC) data, which measures TEC in the direction perpendicular to Earth's surface. The data were obtained from the Madrigal database, accessible at http://madrigal.iggcas.ac.cn/. The temporal resolution of the data is 5 minutes, and the spatial resolution is 1° latitude ×1° longitude. Additionally, geomagnetic activity indices, including the southward component of the interplanetary magnetic field (IMF), solar wind speed, and the symmetric ring current index, were retrieved from the OMNI database at https://omniweb.gsfc.nasa.gov/ow_min.html.

2.2. Processing methods

To extract disturbances from the GPS TEC data, this study employs a filtering method based on residual fitting. The basic process is as follows: a sliding average is applied to the raw data to determine the background trend, which is then subtracted to isolate the TEC disturbances [9, 14, 15].

Assuming that the vertical TEC (VTEC) consists of two components:

$$\mathrm{VTEC} = \mathrm{VTEC}_0 + \mathrm{VTEC}_w$$

The background TEC can be expressed as a second-degree polynomial function of time:

$$\mathrm{VTEC}_0 = C_0 t^2 + C_1 t + C_2$$

Where C_0,C_1 and C_2 are fitting coefficients.

In the specific data processing steps, it was found that the spatial resolution of the data was relatively low. To improve spatial resolution and more clearly display and calculate the propagation characteristics of TIDs, the TEC values at adjacent times were averaged. To ensure the accuracy of the fitted data, it was verified in subsequent steps whether the fitting data coverage exceeded 75%. If

DOI: 10.54254/2755-2721/2025.23742

this condition was met, a two-hour sliding window fitting was performed; otherwise, the data were marked as missing Nan. Finally, the disturbance component VTECw was obtained by subtracting the background $VTEC_0$ from the actual VTEC.

To calculate various parameters of $VTEC_w$, suitable longitude slices were selected [16] to determine the average propagation speed in the longitudinal direction, wave propagation period, start and end times, and average amplitude. The meridional speed was calculated by dividing the latitude change along the line connecting consecutive phase peaks by the corresponding time change. By combining this information with the azimuth angle of the wave observed in the two-dimensional TEC disturbance images, the total average wave speed and wavelength were calculated. This study meticulously observed the propagation of LSTID phase fronts and extracted key parameters, including the propagation speed, wavelength, period, and azimuth of each phase front. These parameters were then used to analyze and discuss the propagation characteristics of LSTIDs.

3. Observational results

3.1. TID observations in the North American Sector during the March 2023 Geomagnetic Storm

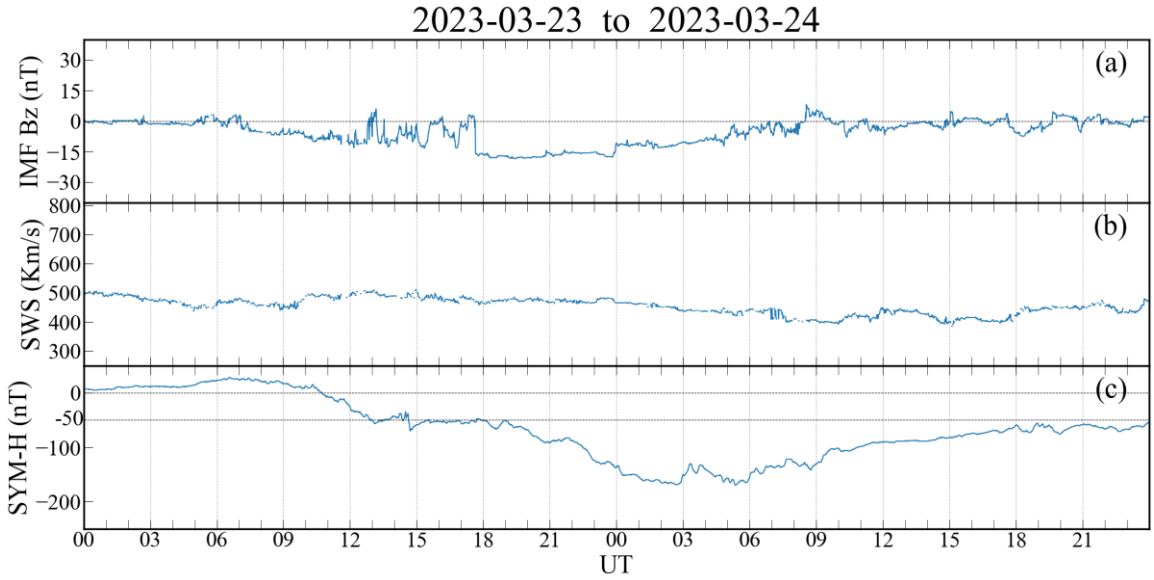

Figure 1: (a) Southward Interplanetary Magnetic Field (IMF), (b) solar wind speed, (c) symmetric ring current index (SYM-H)

According to the monthly summary from the Space Environment Prediction Center (SEPC) (http://www.sepc.ac.cn/archive2.php), the geomagnetic storm event on March 23, 2023, was primarily caused by a coronal mass ejection (CME) on March 20. The initial phase of the storm lasted approximately three hours. Around 13:00 Universal Time (UT), the SYM-H index began to drop to -50 nT, marking the onset of the main phase, which lasted about 14 hours. By approximately 03:00 UT on March 24, the SYM-H index reached its minimum value of approximately -142 nT before entering the recovery phase. During the initial phase of the storm, the southward IMF occasionally switched to a northward orientation, showing enhancements of about 3-5 nT and oscillating between the northward and southward directions. The solar wind speed did not exhibit significant variations during this period.

DOI: 10.54254/2755-2721/2025.23742

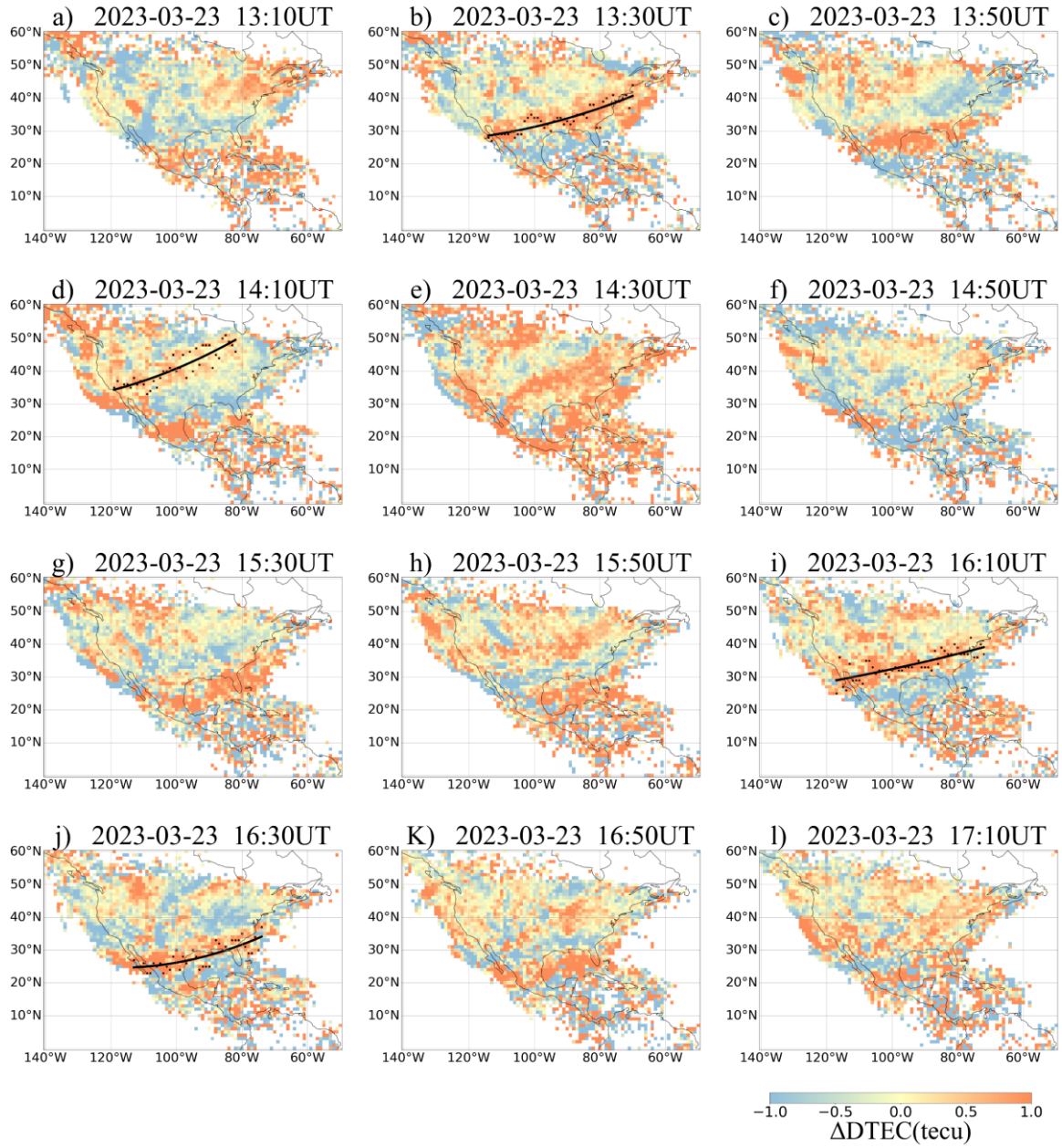

Figure 2: Two-dimensional TEC disturbance maps in the North American Sector from 13:10 to 17:10 UT on March 23, 2023

During the main phase of the geomagnetic storm, three large-scale traveling ionospheric disturbance (LSTID) events propagating from high to low latitudes were observed in the North American sector between 13:10 and 17:10 UT, as shown in Figure 3. Figure 2 (a)-(l) presents the two-dimensional TEC disturbance maps of these LSTIDs. Each map covers a geographical latitude range of 0°-60° N and a longitude range of 50°-140°E, with a temporal resolution of 10 minutes. To illustrate each disturbance event clearly, a 20-minute interval was used for visualization. First Event (13:10-13:50 UT): At 13:10 UT, as shown in Figure 2(a), a clear positive TEC disturbance appeared near 65°-96° E and 35°-50°N. The disturbance phase front propagated equatorward to lower latitudes. By 13:30 UT (Figure 2(b)), the disturbance exhibited a southwest-northeast extension, with an average amplitude of 0.9 TECU and a phase front width of approximately 2,470 km. Positive disturbance points (black points) along the phase front were selected and fitted with a second-order

DOI: 10.54254/2755-2721/2025.23742

polynomial to represent the phase front spatial distribution (black curve). The fitted curve was used to calculate the phase front azimuth and average amplitude, preparing for subsequent velocity calculations. The disturbance continued to propagate equatorward along a direction approximately 9.6° southeast of south, as shown in Figure 2(b). By 13:50 UT, the phase front had nearly dissipated (Figure 2(c)). Second Event (14:30–15:10 UT): As shown in Figures 2(d)–(f), the phase front width reached approximately 2,000 km, with a propagation azimuth of 24° southeast of south, deviating by about 10° from the adjacent event. By analyzing the variation of TEC disturbances with latitude and time in Figure 3, the horizontal longitudinal velocity was estimated. Combining this with the azimuth, the calculated horizontal average velocity was approximately 610 m/s. Third Event (15:50–16:50 UT): At 15:50 UT, as shown in Figures 2(g)–(l), two positive TEC disturbance phase peaks appeared. The southeastward-propagating disturbance was the focus of analysis. This disturbance propagated equatorward along a direction approximately 12° southeast of south, with an average velocity of 512 m/s. The disturbance retained a southwest-northeast orientation and disappeared around 20°N by 16:50 UT.

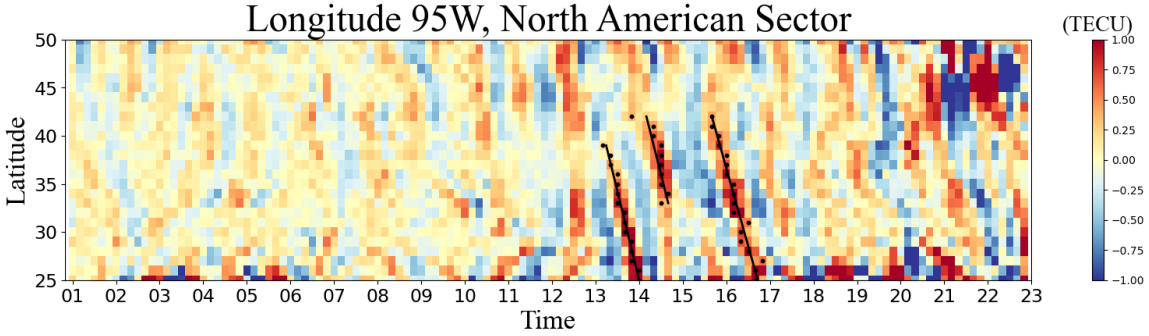

Figure 3: Disturbed TEC as a function of latitude and universal time on March 23, 2023, in the North American Sector

Figure 3 presents a two-dimensional map showing the variation of disturbed TEC with latitude and universal time (UT). To generate this map, three longitude lines (85°W, 95°W, and 105∘W) were selected. The average TEC values within ±5° of each longitude line were computed. Among these, the map with the best visual representation of disturbances was chosen for display [16]. Considering the influence of background TEC variations during the geomagnetic storm, which can be affected by the mid-latitude ionospheric trough, TEC enhancement in the mid- to low-latitude ionosphere, and the equatorial anomaly expanding poleward [17-19], the latitude range for analysis was selected as 25° N to 50° N, based on data coverage and accuracy. From Figure 3, it is evident that the disturbances propagate from high to low latitudes. The statistical results from the analysis are summarized below.

Table 1: LSTID propagation parameters in the North American Sector on March 23, 2023

Measurement Line	Velocity (m/s)	Period (min)	Wavelength (km)	Direction (degrees)	Average Amplitude (TECU)
1	580.95	71	2474.84	南偏东 9.6	0.90
2	610.67	54	1988.95	南偏东 24.4	0.72
3	512.09	80	2458.03	南偏东 12.7	0.82

DOI: 10.54254/2755-2721/2025.23742

3.2. TID observations in the European Sector during the March 2023 Geomagnetic Storm

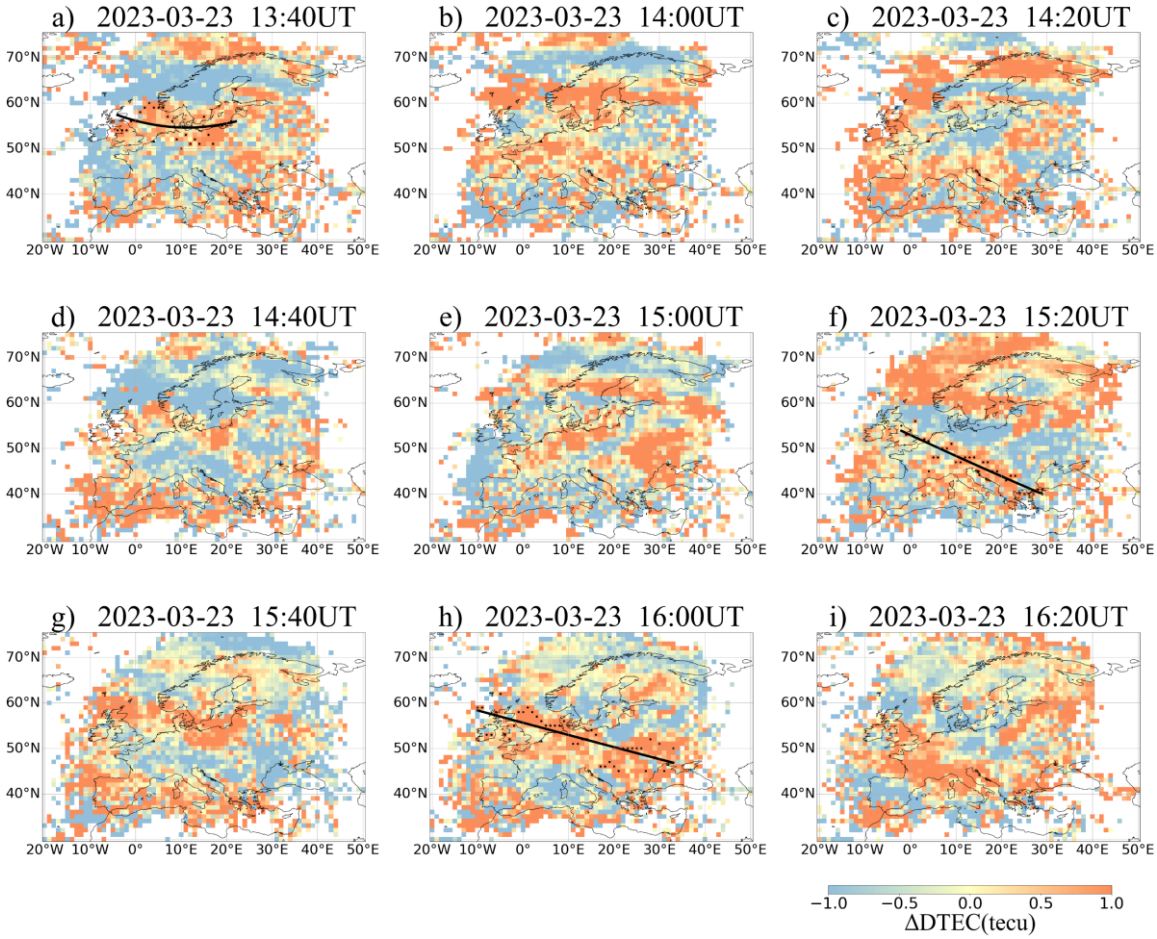

Figure 4: Two-dimensional TEC disturbance maps in the European Sector from 13:40 to 16:20 UT on March 23, 2023

Figure 4 (a)–(i) presents a series of TEC disturbance maps in the European sector during the period from 13:40 to 16:20 UT on March 23, 2023. Each map covers a latitude range of 30° – 75° N and a longitude range of 20°W – 50°E, with a temporal resolution of 10 minutes. To illustrate the disturbance events, a 20-minute interval was used for visualization. During the period from 13:40 to 16:20 UT, significant positive TEC disturbances were observed in the European sector, as shown in Figure 4. At 13:40 UT (Figure 4(a)), a distinct positive disturbance appeared near the geographical longitude range of 5°W–20° E and the latitude range of 50° – 60°N. The average amplitude of this disturbance was 0.85 TECU, and the propagation speed was approximately 620 m/s. The phase front then propagated equatorward in a direction 2.5° southwest of south. Similarly, another significant disturbance occurred in Figures 4(d)–(f). The propagation direction of the disturbance in Figure 4(f) showed a notable change compared to the previous event, with the phase front propagating 31.2° southwest of south. Figures 4(g)–(i) illustrate the third disturbance. The phase front propagated at a speed of 575.38 m/s with a period of approximately 56 minutes. The propagation speeds of the three disturbances were generally consistent, demonstrating a degree of continuity and stability in their characteristics.

DOI: 10.54254/2755-2721/2025.23742

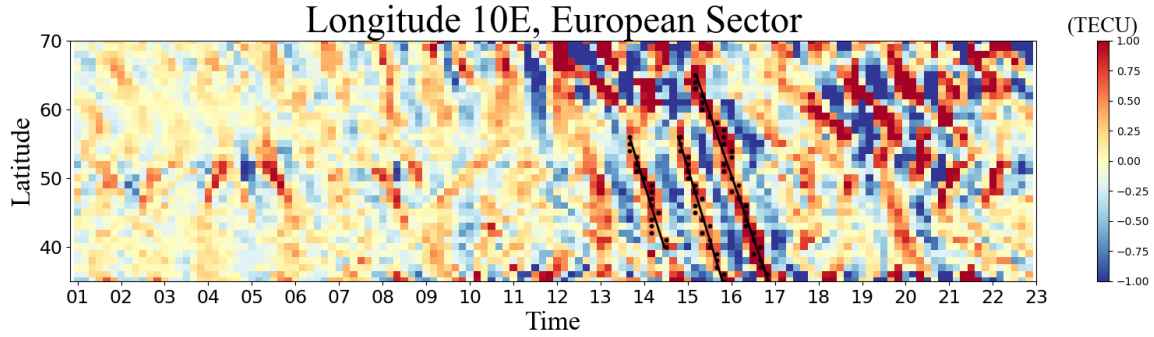

Figure 5: Disturbed TEC as a function of latitude and universal time in the European Sector on March 23, 2023

In Figure 5, peak values of the disturbance were selected, and a linear fitting was performed. The slope of the fitted line was used to calculate the horizontal meridional propagation speed. By combining this with the azimuth angle, the horizontal average speed was calculated. From Figure 5, it is clear that during the period from 13:40 to 16:20 UT, within the latitude range of 35°N–65°N, three disturbance events occurred. The propagation direction for these disturbances was from the polar region toward the equator. By calculating the meridional velocity and azimuth angle, the speeds of the three TIDs were found to range from 570 m/s to 660 m/s. The detailed parameters for the TIDs are provided in Table 2.

Table 2: TID Propagation Parameters in the European Sector on March 23, 2023

Measurement Line	Velocity (m/s)	Period (min)	Wavelength (km)	Direction (degrees)	Average Amplitude (TECU)
1	620.55	71.08	2646.65	South by West 2.5	0.85
2	652.24	58.20	2277.62	South by West 31.2	0.75
3	575.38	56.83	1962.06	South by West 15.1	1.24

4. Conclusion

This study utilized vertical TEC data from the Madrigal database to analyze the morphological characteristics and spatiotemporal evolution of TIDs during the March 2023 geomagnetic storm in the North American and European sectors. The main conclusions are as follows:

During the geomagnetic storm, multiple large-scale traveling ionospheric disturbances (LSTIDs) originating from the Arctic region were observed in the European and North American sectors.

In the initial phase of the geomagnetic storm, intense LSTIDs propagated during the daytime in both the North American and European sectors. The disturbance patterns in the North American sector experienced minimal interference, enabling more wavefronts to be accurately identified.

The propagation speeds of LSTIDs in the North American sector ranged from 512 to 610 m/s, while those in the European sector ranged from 575 to 652 m/s. The average propagation direction of LSTIDs in the North American sector was approximately 15∘15^\circ15∘ southeast of south, whereas in the European sector, the direction averaged 15∘15^\circ15∘ southwest of south.

DOI: 10.54254/2755-2721/2025.23742

Acknowledgments

We would like to express our gratitude to the CEDAR Madrigal database for providing invaluable upper atmosphere science data. Rideout W., Cariglia K. CEDAR Madrigal Database URL: http://cedar.openmadrigal.org

References

[1] *Munro, G. H. (1948). Short-period changes in the F region of the ionosphere. Nature, 162, 886–887.*
[2] *Hines, C. O. (1960). Internal atmospheric gravity waves at ionospheric heights. Canadian Journal of Physics, 38, 1441–1481.*
[3] *Chan, K. L., & Villard Jr, O. G. (1962). Observation of large-scale traveling ionospheric disturbances by spaced-path high-frequency instantaneous-frequency measurements. Journal of Geophysical Research (1896–1977), 67, 973–988.*
[4] *Davis, M. J., & Da Rosa, A. V. (1969). Traveling ionospheric disturbances originating in the auroral oval during polar substorms. Journal of Geophysical Research (1896–1977), 74, 5721–5735.*
[5] *Hunsucker, R. D. (1982). Atmospheric gravity waves generated in the high-latitude ionosphere: A review. Reviews of Geophysics, 20, 293–315.*
[6] *Hocke, K., & Schlegel, K. (1996). A review of atmospheric gravity waves and traveling ionospheric disturbances: 1982–1995. Annales Geophysicae, 14, 917–940.*
[7] *Afraimovich, E. L., Kosogorov, E. A., Leonovich, L. A., Palamartchouk, K. S., Perevalova, N. P., & Pirog, O. M. (2000). Determining parameters of large-scale traveling ionospheric disturbances of auroral origin using GPS-arrays. Journal of Atmospheric and Solar-Terrestrial Physics, 62, 553–565.*
[8] *Saito, A., Fukao, S., & Miyazaki, S. (1998). High resolution mapping of TEC perturbations with the GSI GPS network over Japan. Geophysical Research Letters, 25, 3079–3082.*
[9] *Tsugawa, T., Saito, A., & Otsuka, Y. (2004). A statistical study of large-scale traveling ionospheric disturbances u sing the GPS network in Japan. Journal of Geophysical Research: Space Physics, 109. https://doi.org/10.1029/2003JA010302*
[10] *Ding, F., Wan, W., Liu, L., Afraimovich, E. L., Voeykov, S. V., & Perevalova, N. P. (2008). A statistical study of large-scale traveling ionospheric disturbances observed by GPS TEC during major magnetic storms over the years 2003–2005. Journal of Geophysical Research: Space Physics, 113. https://doi.org/10.1029/2008JA013037*
[11] *Ding, F., Wan, W., Ning, B., & Wang, M. (2007). Large-scale traveling ionospheric disturbances observed by GPS total electron content during the magnetic storm of 29–30 October 2003. Journal of Geophysical Research: Space Physics, 112. https://doi.org/10.1029/2007JA012377*
[12] *Song, Q., Ding, F., Wan, W., Ning, B., & Zhao, B. (2013). Monitoring traveling ionospheric disturbances using the GPS network around China during the geomagnetic storm on 28 May 2011. Science China Earth Sciences, 56, 718–726. https://doi.org/10.1007/s11430-012-4542-7*
[13] *Zhang, S.-R., Erickson, P. J., Coster, A. J., Rideout, W., Vierinen, J., Jonah, O., & Goncharenko, L. P. (2019). Subauroral and polar traveling ionospheric disturbances during the 7–9 September 2017 storms. Space Weather, 17, 1748–1764. https://doi.org/10.1029/2019SW002271*
[14] *Shiokawa, K., Otsuka, Y., Ogawa, T., Balan, N., Igarashi, K., Ridley, A. J., Knipp, D. J., Saito, A., & Yumoto, K. (2002). A large-scale traveling ionospheric disturbance during the magnetic storm of 15 September 1999. Journal of Geophysical Research: Space Physics, 107(SIA 5-1–SIA 5-11). https://doi.org/10.1029/2001JA000245*
[15] *Nicolls, M. J., Kelley, M. C., Coster, A. J., González, S. A., & Makela, J. J. (2004). Imaging the structure of a large-scale TID using ISR and TEC data. Geophysical Research Letters, 31. https://doi.org/10.1029/2004GL019797*
[16] *Zakharenkova, I., Astafyeva, E., & Cherniak, I. (2016). GPS and GLONASS observations of large-scale traveling ionospheric disturbances during the 2015 St. Patrick's Day storm. Journal of Geophysical Research: Space Physics, 121, 12,138–12,156. https://doi.org/10.1002/2016JA023332*
[17] *Mannucci, A. J., Tsurutani, B. T., Iijima, B. A., Komjathy, A., Saito, A., Gonzalez, W. D., Guarnieri, F. L., Kozyra, J. U., & Skoug, R. (2005). Dayside global ionospheric response to the major interplanetary events of October 29–30, 2003 "Halloween Storms". Geophysical Research Letters, 32. https://doi.org/10.1029/2004GL021467*
[18] *Foster, J. C., & Rideout, W. (2005). Midlatitude TEC enhancements during the October 2003 superstorm. Geophysical Research Letters, 32. https://doi.org/10.1029/2004GL021719*
[19] *Basu, S., Basu, S., Groves, K. M., Mackenzie, E., Keskinen, M. J., & Rich, F. J. (2005). Near-simultaneous plasma structuring in the midlatitude and equatorial ionosphere during magnetic superstorms. Geophysical Research Letters, 32. https://doi.org/10.1029/2004GL021678*